PERGAMON

International Journal of Heat and Mass Transfer 43 (2000) 1759–1766

International Journal of HEAT and MASS TRANSFER

www.elsevier.com/locate/ijhmt

Turbulent heat transfer in liquid iron during electron beam evaporation

Ch. Karcher[a,*], R. Schaller[a], Th. Boeck[b], Ch. Metzner[c], A. Thess[b]

[a]*Institute for Aerospace Engineering, Dresden University of Technology, Mommsenstrasse 13, 01062 Dresden, Germany*
[b]*Department of Mechanical Engineering, Ilmenau University of Technology, P.O. Box 100565, 98684 Ilmenau, Germany*
[c]*Fraunhofer Institute for Electron Beam and Plasma Technologies, Winterbergstrasse 28, 01277 Dresden, Germany*

Received 17 June 1998; received in revised form 4 August 1999

Abstract

Electron beam evaporation of high-purity liquid metals is characterized by vigorous (turbulent) convection in the melt pool resulting in unwelcome heat losses. This convective motion is exclusively driven by thermocapillary forces. We exploit this unique feature to measure the Nusselt number in liquid iron for Marangoni numbers up to 10^8. The experiments are carried out in a real-to-life test facility for electron beam evaporation. We compare the results of our investigations with findings of a recent scaling analysis. Moreover, we perform direct numerical simulations employing a 2D model. The numerical results demonstrate the turbulent character of the flow as well as the dominance of thermocapillarity over buoyancy. © 2000 Elsevier Science Ltd. All rights reserved.

Keywords: Heat transfer; Liquid metals; Thermocapillary

1. Introduction

Electron beam evaporation of metals is an innovative technology increasingly used in industry to produce very thin (<1 μm) coatings of high purity (cf. Schiller et al. [1]). In this process, the surface of a metal ingot is heated by bombardment with a high-energy electron beam gun. The material melts, forming a free surface and eventually starting to evaporate. Fig. 1 shows a principal sketch of the arrangement. The rising vapor cloud condenses as a thin film on a rapidly moving substrate located at some distance above (not shown in Fig. 1). To guarantee a superior quality of the coating, the melt is typically confined in a water-cooled copper crucible of large aspect ratio R/H. Water-cooling is necessary to avoid chemical reactions between melt and crucible material.

The strong energy flux from the electron beam ($Q_B \approx 50$ kW) induces strong temperature gradients along the free surface and in the interior of the melt. Hence, the liquid metal is subject to both surface-tension-driven (thermocapillary) convection (cf. Davis [2]) and buoyancy-driven convection (cf. Siggia [3]). However, for the actual arrangement of Fig. 1 (heated from above, large aspect ratio R/H), various numerical and analytical studies show that (turbulent) thermocapillary convection is the dominant mode of heat transfer, see e.g. Karcher [4], Pumir and Blumenfeld [5], DebRoy and Davis [6], Avare [7]. This conclusion is also supported by our present numerical investigations. The strong convective heat transfer limits the temperature rise at the free surface and therefore the thermodyn-

* Corresponding author. Tel.: +49-351-463-8095; fax: +49-351-463-8087.
E-mail address: karcher@tfd.mw.tu-dresden.de (C. Karcher).

0017-9310/00/$ - see front matter © 2000 Elsevier Science Ltd. All rights reserved.
PII: S0017-9310(99)00248-3

Nomenclature

c_p	heat capacity of liquid	S, V	free surface area, volume
g	acceleration of gravity	t	time
H	height of crucible, characteristic length of heat transfer	T	temperature
		T^*	averaged surface temperature
R	radius of crucible	T_M	melting temperature
Ma	Marangoni number	u, v, w	velocity components
Nu	Nusselt number	$\mathbf{v}$	velocity vector
p	pressure	$\mathbf{v}_H$	horizontal velocity vector
Pr	Prandtl number		
q_B	absorbed electron beam power density	*Greek symbols*	
Q_B	electron beam power	α	coefficient of thermal expansion
Q	power in coolant, absorbed electron beam power	γ	temperature coefficient of surface tension
		κ, κ_t	molecular diffusivity, turbulent diffusivity
r, z	axisymmetric coordinates	λ	thermal conductivity
r_B	characteristic radius of electron beam	ν, ν_t	molecular viscosity, turbulent viscosity
Ra	Rayleigh number	ρ	density

amic efficiency of the evaporation process. In typical applications, only a small portion of about 3% of the electron beam power input is converted into vapor energy [1]. The present study therefore aims to contribute to the physical understanding of the turbulent heat transfer in purely surface-tension-driven convection at high Marangoni numbers in a melt heated at its free surface. Our investigations include real-to-life experiments in a test facility for the evaporation of metals. The findings shall be compared on a qualitative basis with predictions of recently proposed scaling analyses [4,5] for heat transfer in fully developed turbulent thermocapillary convection. Furthermore, we perform direct numerical simulations of the process to attain a qualitative picture of the flow features.

The present report is organized as follows. In Section 2 we show the governing equations and boundary conditions of the problem. We also briefly recall the analysis leading to the basic scaling law of heat transfer. In Sections 3 and 4 we present results of our experimental and numerical investigations, respectively. Finally, in Section 5 we summarize the main findings.

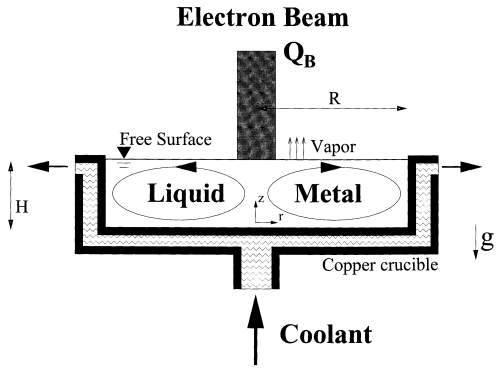

Fig. 1. Principle sketch of the arrangement.

2. Governing equations and scaling analysis

2.1. Governing equations

Consider the axisymmetric arrangement as sketched in Fig. 1. The governing equations drawn up below are derived under the following assumptions:

1. the material inside the crucible is all liquid;
2. the liquid is incompressible and obeys the Boussinesq approximation (cf. Ref. [8]);
3. the effect of bouyancy is neglected;
4. the free surface is nondeformable;
5. for reasons of transparency the contributions of thermal radiation (typically less than 10% [1]) and evaporation (less than 3%) to the energy balance at the free surface are not considered.

Within these assumptions the conservation equations for mass, momentum, and energy in the liquid read as follows. In vector notation we obtain

$$\nabla \cdot \mathbf{v} = 0, \tag{1a}$$

$$\left(\frac{\partial}{\partial t} + (\mathbf{v}\cdot\nabla)\right)\mathbf{v} = -\frac{1}{\rho}\nabla p + \upsilon\nabla^2\mathbf{v}, \tag{1b}$$

$$\left(\frac{\partial}{\partial t} + (\mathbf{v}\cdot\nabla)\right)T = \kappa\nabla^2 T. \tag{1c}$$

Here the variables of state are the velocity vector $\mathbf{v}$, the pressure p, and the temperature T. The constant fluid properties are the density ρ, the kinematic viscosity υ, and the thermal diffusivity κ. Shear stress and energy balance at the free surface ($z=H$) along with the kinematic condition yield the relations

$$\frac{\partial \mathbf{v}_{\mathrm{H}}}{\partial z} = -\frac{\gamma}{\rho\nu}\nabla T \quad \text{at } z = H, \tag{2a}$$

$$\lambda\frac{\partial T}{\partial z} = q_{\mathrm{B}}(r) = q_0 \exp\{-r^2/2r_{\mathrm{B}}^2\} \quad \text{at } z = H, \tag{2b}$$

$$w = 0 \quad \text{at } z = H. \tag{2c}$$

Here, γ ($\gamma > 0$) is the thermal coefficient of surface tension and λ is the thermal conductivity of the fluid. Moreover, in Eq. (2b) q_{B} is the power density from the electron beam absorbed by the liquid metal. It is assumed that the beam has a Gaussian distribution with the characteristic radius r_{B}. The set of boundary conditions is completed by no-slip ($\mathbf{v}=0$), fixed-temperature ($T=T_{\mathrm{M}}$) conditions at the crucible walls at $z = 0$ and $r=\pm R$.

2.2. Scaling analysis

A detailed analysis leading to the basic scaling law of turbulent heat transfer in a liquid heated at its free surface was performed independently by Karcher [4] and Pumir and Blumenfeld [5]. In the present paper, we therefore give only a brief summary of this analysis. We multiply Eqs. (1b,c) by $\mathbf{v}$ and T, respectively, and average over the entire domain. Integrating by parts and using boundary conditions (Eqs. (2a–c)) we derive the following equations that describe the steady-state balance of production of kinetic and thermal energy at the free surface (S) and dissipation in the volume (V):

$$\frac{1}{\rho c_{\mathrm{p}}}\int_{(S)} q_{\mathrm{B}} T \,\mathrm{d}S = \kappa_{\mathrm{t}}\int_{(V)} (\nabla T)^2 \,\mathrm{d}V, \tag{3a}$$

$$-\frac{\gamma}{\rho}\int_{(S)} \mathbf{v}_{\mathrm{H}}\cdot\nabla T \,\mathrm{d}S = \nu_{\mathrm{t}}\int_{(V)} (\nabla\times\mathbf{v})^2 \,\mathrm{d}V, \tag{3b}$$

where $\mathbf{v}_{\mathrm{H}}$ denotes the horizontal velocity vector. In fully developed turbulent flow, the diffusivities can be assumed to be of the eddy type (please note subscript t in Eqs. (3a,b)). These quantities depend only on the characteristic macroscopic velocity (u) and on the characteristic macroscopic length scale (H, see below) of the problem; cf. Landau and Lifshitz [9]. A dimension analysis implies the scaling relations

$$\kappa_{\mathrm{t}} \propto uH, \tag{4a}$$

$$\nu_{\mathrm{t}} \propto uH. \tag{4b}$$

To evaluate Eqs. (3) and (4) qualitatively we introduce the following scales:

$$r \propto R, \tag{5a}$$

$$z \propto H, \tag{5b}$$

$$S \propto R^2, \tag{5c}$$

$$V \propto HR^2, \tag{5d}$$

$$T \propto (q_0 H)/\lambda, \tag{5e}$$

$$u \propto \kappa/H. \tag{5f}$$

Note that this scaling accounts for varying aspect ratios R/H. Therefore, the present approach extends the analysis of Pumir and Blumenfeld [5], which assumes that R and H are of the same order of magnitude. As the characteristic length scale of the present heat transfer problem we define the liquid layer height H. This choice is consistent with the large aspect ratio R/H of the crucible actually used in the experiments, cf. Section 3. In this case we can assume that the large scale flow consists of convection rolls with characteristic dimension H. This assumption is supported by the results of our numerical investigations, cf. Fig. 5 in Section 4. We combine Eqs. (3)–(5) to finally obtain the general scaling law

$$Nu \propto \left(Ma\, Pr\frac{H}{R}\right)^{1/3}. \tag{6}$$

The dimensionless groups, the Nusselt number Nu, the Marangoni number Ma, and the Prandtl number Pr are defined as follows:

$$Nu = \frac{Q}{H\lambda(T^* - T_{\mathrm{M}})}, \tag{7a}$$

$$Ma = \frac{\gamma Q}{\rho\nu\kappa\lambda}, \tag{7b}$$

$$Pr = \frac{\nu}{\kappa}, \tag{7c}$$

where T^* denotes the averaged surface temperature. Moreover, Q is the power actually absorbed at the free surface and transported through the layer. This quantity is controlled in experiment. Hence, to evaluate Eq. (7a) our goal shall be to measure T^* for a given value of Q.

3. Experiments

The main goal of the present numerical investigations is to determine the dependence of the Nusselt number on the Marangoni number in parameter regimes that are not accessible in conventional laboratory experiments. The results shall be compared to the prediction of the scaling analysis, cf. Eq. (6). We focus on the evaporation of liquid iron ($Pr \approx 0.01$) which is a material typically used in application [1]. The effect of the aspect ratio on the heat transfer was investigated numerically by Karcher et al. [10].

Fig. 2 shows a schematic view of the experimental test facility used for the evaporation of metals. The process requires a high-vacuum environment of $p \cong 10^{-4}$ hPa; cf. Ref. [1]. The test material is iron confined in a cylindrical copper crucible of aspect ratio $R/H = 82.5$ mm/20 mm. The electron beam gun generates a maximal power of $Q_B = 50$ kW. With this actual set-up we are able to realize Marangoni numbers up to 10^8. During the experiments we measure the beam power Q_B, the power in the coolant Q (cf. Eqs. (7a,b)), and the temperature at the inner crucible wall at about half the height. Moreover, the temperature of the free surface of the molten iron is measured using an infra-red camera. A pivoting shutter prevents the optical path of the camera from steaming up. The results of in situ measurements of the evaporation rate and the surface movement will be reported elsewhere [11].

Fig. 3 shows the results of a typical experimental run in which the power of a focused electron beam ($r_B = 1$ cm) is increased from $Q_B = 5$ up to 50 kW in increments of 5 kW. The actual increase of Q_B is carried out after the response signal for Q has leveled out. We observe that upon increasing Q_B, the power in the coolant Q also increases proportionally. The difference between the two powers is mainly caused by back-scattering of electrons ($\approx 40\%$ for iron, cf. Ref. [1]) at the surface of the melt. On the other hand, from the signal of a thermocouple, placed at mid-height of the inner crucible wall, we conclude that the iron inside the crucible is not completely molten ($T_M = 1536°C$). Instead, a melt puddle forms. Furthermore, since the temperature signal remains almost constant for $Q_B > 25$ kW, we conclude that the puddle does not change its length for higher heating powers. Moreover, the signal shows large fluctuations in this parameter range. We attribute this feature to the vigorous convective motion in the melt. These conclusions are also supported by the measurements of the surface temperature of the melt puddle, see the snapshot given in Fig. 4. In this case the electron beam power is fixed at $Q_B = 40$ kW. The diameter of the melt puddle is about 2/3 of the horizontal dimension of the crucible. The surface temperature decreases nonuniformly in radial direction from the hot spot in the center ($T = 2500°C$) to the outer boundary of the free surface of the puddle ($T = 2170°C$). We conclude that the nonuniform temperature fall is due to turbulent motion in the melt. As observed with a video camera, the typical surface vel-

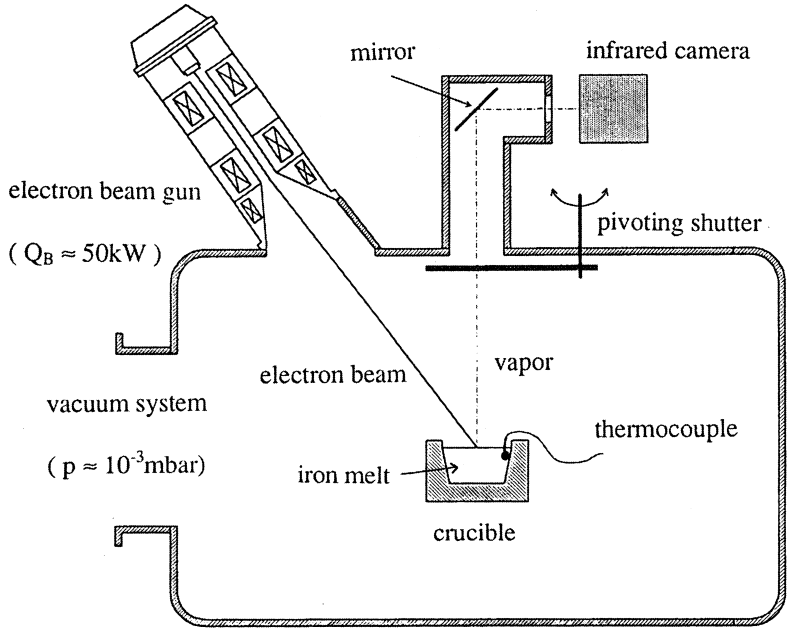

Fig. 2. Schematic view of the test facility for electron beam evaporation of liquid metals.

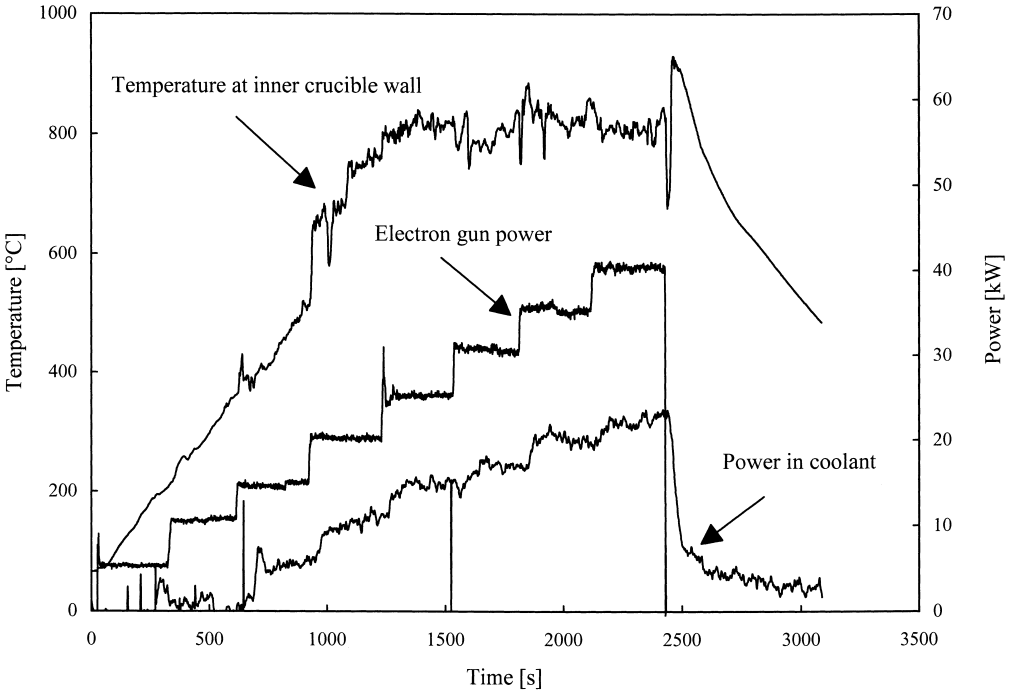

Fig. 3. Example of a typical run. The electron beam power Q_B is increased from 5 to 40 kW in increments of 5 kW. Recorded are the electron beam power, the power in the coolant Q, and the temperature at the inside of the crucible wall.

ocity is 0.1 m/s. This corresponds well to the observed dynamic time scale of the isotherms of about 1 s. At the outer boundary (cf. Fig. 4), the surface temperature drops within a thin layer to the melting temperature. This gives rise to the formation of a thermal boundary layer in this region. The surface of this layer is covered with slag particles (ferric oxide) having a different emissivity than the free surface of the melt pool. Hence, this region cannot be resolved during the actual measurements. A summary of the experimental data, showing the dependence of the Nusselt number on the Marangoni number, is given in Fig. 7.

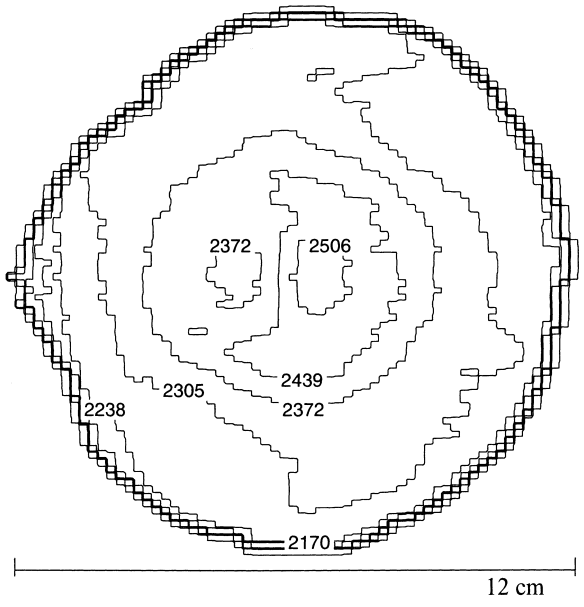

Fig. 4. Snapshot with an infrared camera of the surface temperature in an iron melt pool for an electron beam power of 40 kW. Temperatures are given in °C.

4. Direct numerical simulations

The main objective of our direct numerical simulations is to obtain more insight into the dynamics of heat transfer triggered by thermocapillary convection in a melt heated at its free surface. For the present computations we therefore make the same assumptions as in the analysis shown in Section 2. However, the actual simulations are carried out in a two-dimensional Cartesian domain rather than in a 3D cylindrical box. This simplification is necessary to reach the high Marangoni numbers under consideration. Moreover, in contrast to the analysis we apply free-slip, adiabatic boundary conditions in lateral direction. Nevertheless, we think that our 2D approach also permits us to test

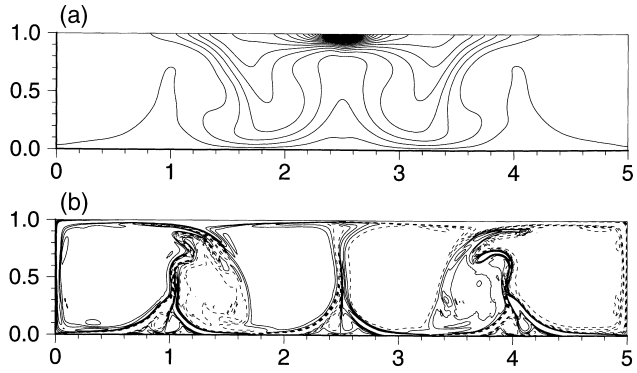

Fig. 5. Direct numerical simulation of two-dimensional Marangoni convection for $Ma = 1.38 \times 10^5$, $Pr = 10^{-2}$, $R/H = 5$, and $r_B/R = 1/16$. The boundary conditions are free-slip, adiabatic side walls and a no-slip, perfectly conducting bottom. Snapshots of the temperature field (a) and the vorticity field (b).

qualitatively the predictions of the scaling analysis. The employed code uses a spectral spatial discretization with Fourier series in the horizontal r-direction and a Chebyshev polynomial expansion in the vertical z-direction; see Ref. [12] for details. Throughout the simulations we fix parameters at $R/H = 5$, $Pr = 0.01$, and $r_B/R = 1/16$.

Fig. 5 shows snapshots of the temperature field (Fig. 5a) and the vorticity field (Fig. 5b) for $Ma = 1.38 \times 10^5$, the highest value that was reached in the simulations. Hence, in the simulations the typical Marangoni number is two to three orders of magnitude less than in the experiments. Fig. 5a shows that the isotherms are strongly compressed right beneath the heated part of the surface. This demonstrates that a thermal boundary layer forms in this region. Moreover, the strong distortion of the isotherms in vertical direction clearly shows that surface-tension-driven convection strongly increases the heat transfer across the liquid layer. In particular, the vorticity field (Fig. 5b) displays that the flow pattern consists of three pairs of convection rolls that occupy the entire height of the layer. Due to the Marangoni effect, primary vorticity is produced at the free surface pushing fluid in a jet-like stream from the hot center part to the colder outer regions. By continuity, this interfacial mass transport generates an upflow right below the hot spot. On the other hand, the jet flows down the free-slip side walls but separates at the rigid bottom boundary. There, secondary vorticity is produced and transported into the bulk, generating a counter-rotating secondary convection roll. This separation phenomenon splits the jet at the free surface and, therefore, limits the interfacial temperature drop to the region occupied by the inner convection roll, cf. Fig. 5a. Please note that the lateral symmetry in Fig. 5 is sometimes strongly perturbed due to symmetry-breaking events occurring spontaneously in the course of the simulation. The spatio-temporally irregular behavior of the flow can be viewed in a video sequence at our web page.[1] In Fig. 6 we have plotted the Nusselt number according to Eq. (6a) versus time. The random fluctuations in the Nusselt number of about 10% indicate that the system is in a turbulent state. Moreover, the time-averaged value of $Nu = 61.5$ supports our earlier conclusion, namely that in the present problem turbulent thermocapillary convection is the dominant mode of heat transfer. For comparison, we have also calculated the Nusselt number for the case of purely buoyancy-driven convection for a corresponding Rayleigh number of $Ra = (\alpha g Q H^2)/(\lambda \kappa \nu) = 10^7$. In this case it turns out that the Nusselt number is of order one, being only slightly greater than the value for pure conduction. Please note that the used temperature scale results in $Nu \propto O(1)$ but $Nu \neq 1$ for the conductive state. The results of our direct numerical simulations for a series of Marangoni numbers are summarized in Fig. 7.

5. Conclusions

We have investigated both experimentally and numerically the heat transfer in surface-tension-driven convection in liquid iron heated at its free surface for Marangoni numbers typical in electron beam evaporation. The findings are tested and compared qualitatively with results of a scaling analysis which predicts the law $Nu \propto Ma^{1/3}$ for turbulent flow. Fig. 7 shows a summary of our studies. The experiments, performed in an electron beam evaporator, span the range $2 \times 10^7 \leq Ma \leq 10^8$. In this range the data yield the dependence $Nu \propto Ma^{0.30 \pm 0.06}$, i.e. the real-to-life test facility has a reasonable reproducibility of $\pm 20\%$, cf. error

[1] www.tu-dresden.de/mwilr/ik/publ.html.

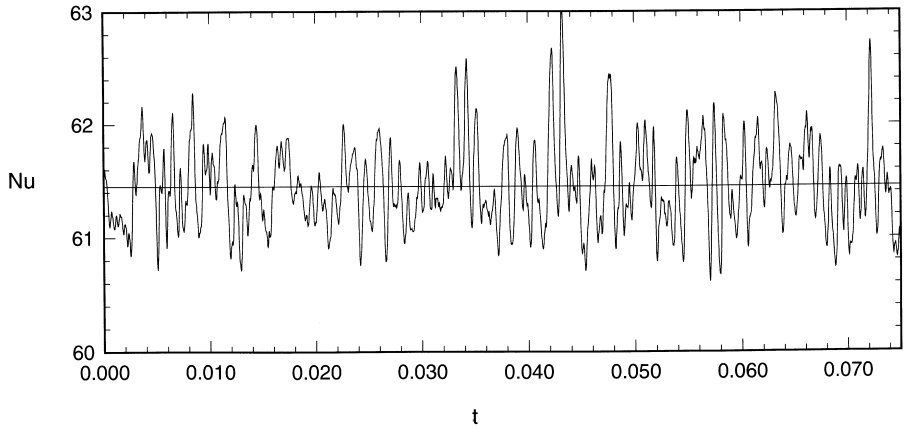

Fig. 6. Temporal evolution of the Nusselt number. Parameters are the same as in Fig. 5. The random fluctuations show that the system is in a state of turbulent convection.

bars in Fig. 7. We conclude that the difference of about 10% between the predicted and the measured exponent is caused by the simplifying assumptions made in the scaling analysis. For instance, assumptions (i) and (iv), i.e. that the metal in the crucible is completely molten and that the free surface remains flat, clearly do not hold in the experiments. On the other hand, in the direct numerical simulations we are able to investigate the range $7 \times 10^4 \leq Ma \leq 1.4 \times 10^5$. In this range the simulations show a dependence according to the relation $Nu \propto Ma^{0.27}$. We conclude that the difference to the analytical prediction is due to the use of a 2D model in the computational approach rather than a 3D one.

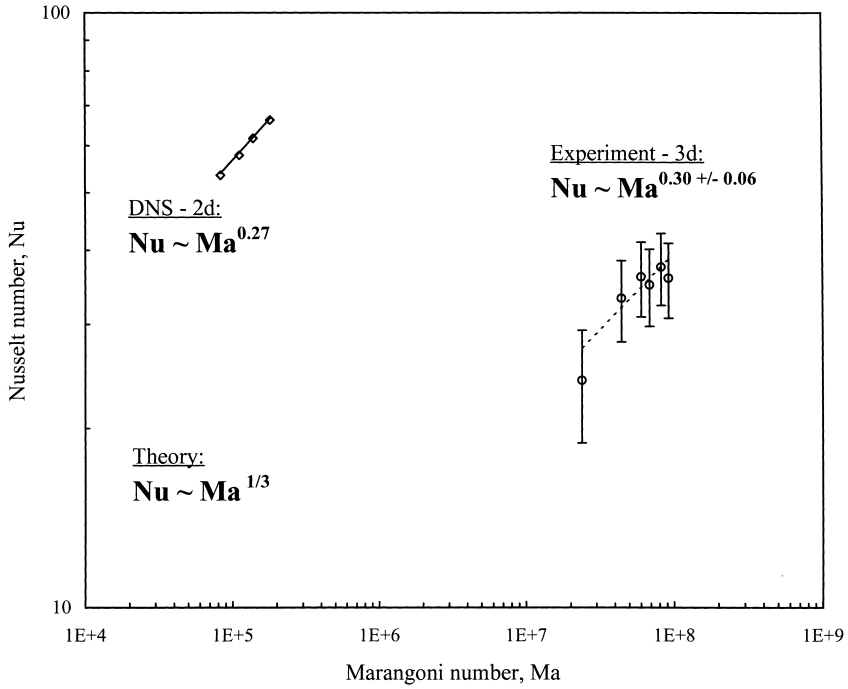

Fig. 7. Dependence of the Nusselt number on the Marangoni number. Results of the 2D direct numerical simulations (left curve) and 3D experiments (right curve). The error bars on the data indicate an experimental reproducibility of 20%.

Acknowledgements

This work was sponsored by the Deutsche Forschungsgemeinschaft under Grants INK18/C3.1 and C3.2. The authors are grateful to the participants of the international workshop on 'Hydrodynamic aspects of electron beam technologies', held in spring 1997 in Dresden, for useful comments and fruitful discussions. Moreover, we are grateful to H. Kern for operating the electron beam evaporator.

References

[1] S. Schiller, U. Heisig, S. Panzer, Electron Beam Technology, John Wiley and Sons, New York, 1982.
[2] S.H. Davis, Thermocapillary instabilities, Ann. Rev. Fluid Mech. 19 (1987) 403–435.
[3] E.D. Siggia, High Rayleigh number convection, Ann. Rev. Fluid Mech. 26 (1994) 137–168.
[4] Ch. Karcher, Electron beam evaporation of metals: scaling analysis and numerical simulation, Work report B 911, Dresden University of Technology, 1996.
[5] A. Pumir, L. Blumenfeld, Heat transport in a liquid layer locally heated on its free surface, Phys. Rev. E 54 (1996) 4528–4531.
[6] T. DebRoy, S.A. David, Physical processes in fusion welding, Rev. Mod. Phys. 67 (1995) 85–112.
[7] Ch. Avare, Etude et modélisation de l'effet thermocapillaire, application à la refusion des métaux réfractaires, Ph.D. thesis, L'Institut Nationale Polytechnique de Grenoble, Grenoble, 1994.
[8] J. Platten, J. Legros, Convection in Liquids, Springer-Verlag, New York, 1984.
[9] L.D. Landau, E.M. Lifshitz, Course of Theoretical Physics, Fluid Mechanics, vol. 6, Pergamon Press, New York, 1987.
[10] Ch. Karcher, R. Schaller, A. Thess, Convective heat transfer during electron beam evaporation of liquid metals, in: N. El-Kaddah (Ed.), Fluid Flow Phenomena in Metals Processing, TMS Publication, Warrendale, 1999.
[11] R. Schaller, Ch. Karcher, A. Thess, Electron beam evaporation of iron confined in a water-cooled crucible, J. Vac. Sci. (1999) (submitted).
[12] Th. Boeck, A. Thess, Inertial Benard–Marangoni convection, J. Fluid Mech. 350 (1997) 149–175.